

KVSlimmer: Theoretical Insights and Practical Optimizations for Asymmetric KV Merging

Lianjun Liu¹ Hongli An² Weiqi Yan³ Xin Du⁴ Shengchuan Zhang³ Huazhong Liu⁴ Yunshan Zhong^{4*}

Abstract

The growing computational and memory demands of the Key-Value (KV) cache significantly limit the ability of Large Language Models (LLMs). While KV merging has emerged as a promising solution, existing methods that rely on empirical observations of KV asymmetry and gradient-based Hessian approximations lack a theoretical foundation and incur suboptimal compression and inference overhead. To bridge these gaps, we establish a theoretical framework that characterizes this asymmetry through the spectral energy distribution of projection weights, demonstrating that concentrated spectra in Query/Key weights induce feature homogeneity, whereas dispersed spectra in Value weights preserve heterogeneity. Then, we introduce KVSlimmer, an efficient algorithm that captures exact Hessian information through a mathematically exact formulation, and derives a closed-form solution utilizing only forward-pass variables, resulting in a gradient-free approach that is both memory- and time-efficient. Extensive experiments across various models and benchmarks demonstrate that KVSlimmer consistently outperforms SOTA methods. For instance, on Llama3.1-8B-Instruct, it improves the LongBench average score by 0.92 while reducing memory costs and latency by 29% and 28%, respectively.

1. Introduction

Large Language Models (LLMs) are increasingly tasked with processing long contexts for applications such as multi-

¹School of Information and Communication Engineering, Hainan University, Haikou, China ²School of Cyberspace Security, Hainan University, Haikou, China ³MAC Lab, Department of Artificial Intelligence, School of Informatics, Xiamen University, Xiamen, China ⁴School of Computer Science and Technology, Hainan University, Haikou, China. Correspondence to: Yunshan Zhong <yszhong01@gmail.com>.

Preprint. March 3, 2026.

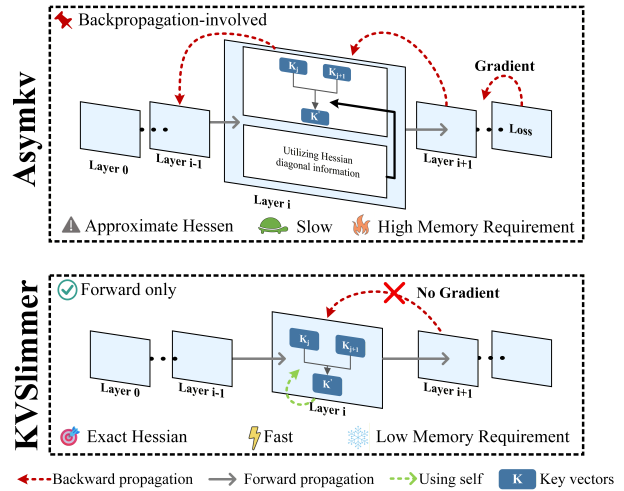


Figure 1. Comparison between AsymKV and KVSlimmer for KV cache merging.

step tool usage, retrieval-augmented generation based on multi-document corpora, chain-of-thought style reasoning, coding agents, and so on (Wang et al., 2024a; Liu et al., 2025c; Huang et al., 2024; Liu et al., 2025a). However, as the context length extends, the quadratic computational growth of the attention mechanism and the linear expansion of the Key-Value (KV) cache storage (Dao et al., 2022; Keles et al., 2022) create a severe memory bottleneck, hindering the practical deployment of LLMs for ultra-long sequences.

To mitigate this, KV cache compression has emerged as a pivotal solution. Existing approaches primarily fall into two categories: eviction and merging. Eviction methods (Zhang et al., 2023; Liu et al., 2023a; Ge et al., 2024; Xiao et al., 2024b) prune tokens deemed less important, but risk discarding information critical for future predictions. Merging methods (Zhang et al., 2024; Liu et al., 2024a; Wang et al., 2025b; Wan et al., 2025), which combine multiple tokens into condensed representations, offer a more information-preserving alternative.

While conventional KV merging methods often apply identical operations to Keys and Values, the recent AsymKV (Cui & Xu, 2025) empirically revealed a critical asymmetry: adjacent Keys exhibit high homogeneity, whereas adjacent

Values remain markedly heterogeneous. Building on this insight, AsymKV employs an approximate Hessian that relies on gradient backpropagation for adjacent Keys merging. Nevertheless, it leaves several critical avenues for further investigation: (1) the lack of a theoretical explanation for this asymmetry, (2) an incomplete second-order Hessian approximation that neglects off-diagonal Key couplings, and (3) a practical dependence on backpropagation, incurring inference overhead.

To bridge these gaps, we first establish a unified spectral analysis framework to uncover the origins of QKV (dis)similarity. Our analysis demonstrates that the homogeneity is fundamentally dictated by the spectral energy distribution of the projection weight, where the concentrated spectral energy in Q/K projections induces homogeneity, whereas the dispersed energy in V projections induces heterogeneity. Then, we propose KVSlimmer a theoretically grounded and computationally efficient framework for asymmetric KV cache merging. As shown in Fig. 1, KVSlimmer derives the exact Hessian to explicitly capture the off-diagonal coupling between adjacent Keys and, more importantly, eliminates the need for backpropagation by deriving a closed-form solution that relies solely on forward-pass variables. This results in a gradient-free, memory- and time-efficient merging algorithm that is both mathematically precise and practically lightweight. Among them, Fig. 1 illustrates the differences between KVSlimmer and AsymKV. Extensive experiments across multiple models and benchmarks demonstrate that KVSlimmer consistently outperforms existing SOTA methods. For instance, when applying KVSlimmer on Llama3.1-8B-Instruct with a chunk_size of 512, it improves the LongBench average score by 0.92 while still reducing memory costs and latency by 29% and 28%, respectively.

2. Related Work

2.1. Long-context Segmentation and Sliding

As a popular KV compression paradigm, long-context segmentation methods partition the context into multiple segments and retain long-range information dependencies by cross-segment recurrence (Dai et al., 2019) or by explicit memory (Rae et al., 2020). RMT (Bulatov et al., 2022) strengthens cross-chunk integration by adopting memory tokens to deliver long-range information. Another paradigm is long-context sliding (Zaheer et al., 2020; Ainslie et al., 2020), which controls KV overhead by adopting local-window attention or sparse attention within each chunk. Longformer (Beltagy et al., 2020) combines sliding-window attention with a small set of global tokens, forming an efficient baseline for long-document modeling. Recent studies (Zhu et al., 2024; Wu et al., 2025) improve the practicality and stability of segmentation and sliding at inference

time. StreamingLLM (Xiao et al., 2024b) stabilizes sliding-window inference via a fixed set of initial KV tokens, known as attention sinks. DCA (An et al., 2024) decomposes attention into intra-block and inter-block modules to achieve training-free long-context extension. InfLLM (Xiao et al., 2024a) extrapolates to long contexts by leveraging efficient context memory and retrieval mechanisms. In addition, CoCA (Zhu et al., 2024) improves boundary behaviors in long-context extrapolation by addressing the coupling between positional encoding and attention. TokenSelect (Wu et al., 2025) selectively involves a few critical KV in attention calculation to reduce inference cost.

2.2. KV cache eviction.

KV eviction methods reduce the computational load and memory footprint during the decoding process initially (Gu et al., 2025b; Kim et al., 2025; Chitty-Venkata et al., 2025; Wang et al., 2025a; Liu et al., 2023b). Subsequently, the focus has gradually shifted towards importance-based KV eviction strategies. H₂O (Zhang et al., 2023) identifies and prioritizes the KV with high contribution evaluated by accumulated attention scores. Subsequently, Scissorhands (Liu et al., 2023b) further introduces the “importance persistence” assumption, retaining KV tokens in a probabilistic manner under a fixed cache budget. Another series of methods moves the eviction decision forward to the prefill phase. For example, SnapKV (Li et al., 2024) and FastGen (Ge et al., 2023) estimate the long-term contribution of prompt tokens through observation windows and attention head differences, respectively. To maximize the utilization efficiency under limited budgets, PyramidKV (Cai et al., 2025) and HeadKV (Fu et al., 2025) introduce layer- and head-level budget allocation strategies. However, as KV eviction methods rely on historical importance estimates to permanently discard tokens, they fail to account for the temporal dynamic nature of token importance, where tokens historically deemed insignificant can become pivotal for future predictions (Gu et al., 2025a; Feng et al., 2025a;b).

2.3. KV Cache Merging.

KV merging methods aggregate multiple historical KV tokens into fewer representations, reducing the KV overhead while still retaining more contextual information for future predictions (Łańcucki et al., 2025; Brandon et al., 2024; Yuan et al., 2025; Li et al., 2025b; Wang et al., 2024b). CaM (Zhang et al., 2024) aggregates KV tokens by employing the ratio of attention scores as merging weights, ensuring that historical importance is preserved within the compressed representation. DMC (Nawrot et al., 2024) learns to decide during generation whether to write new entries to the cache or merge them with existing cache entries, adaptively controlling compression intensity across different layers and heads. For long-context understanding

evaluation, KVMerger (Wang et al., 2025b) models the identification of merge token sets as a constrained clustering problem and employs a kernel-weighted merging strategy. D₂O (Wan et al., 2025) dynamically optimizes KV cache size at both the layer- and token-level. Most existing KV merging methods assume they are functionally equivalent and apply a unified merging strategy to both of them (Li et al., 2025a; Tian et al., 2025; Chang et al., 2025; Liu et al., 2025b). But the recent AsymKV (Cui & Xu, 2025), going beyond a unified strategy, empirically uncovers a structural asymmetry within the adjacent KV cache, where Keys exhibit high homogeneity while Values remain heterogeneous. Based on this finding, AsymKV mathematically proposes a Hessian-based merging strategy that fuses redundant Keys and lossless cardinality normalization for Values merging.

3. Root of KV Asymmetry

3.1. Preliminary

In this subsection, we briefly review AsymKV (Cui & Xu, 2025), a recent KV merging method that serves as a starting point for our KVSlimmer. AsymKV is motivated by the empirical observation that adjacent Keys typically exhibit high homogeneity, while adjacent Values are markedly heterogeneous. Consequently, it proposes a Hessian-based non-uniform merging strategy specifically for adjacent Keys. Given a sequence of Keys $\mathbf{K} = [\mathbf{k}_1, \dots, \mathbf{k}_n]$, AsymKV aims to merge adjacent $(\mathbf{k}_m, \mathbf{k}_{m+1})$ into a single Key \mathbf{k}^* . To determine the optimal \mathbf{k}^* , it minimizes the following loss:

$$\mathbf{k}^* = \arg \min_{\mathbf{k}} \mathcal{L}(\mathbf{k}, \mathbf{k}), \quad (1)$$

where $\mathcal{L}(\mathbf{k}, \mathbf{k})$ denotes the loss when the $(\mathbf{k}_m, \mathbf{k}_{m+1})$ is replaced by (\mathbf{k}, \mathbf{k}) . To solve this optimization problem, a second-order Taylor expansion is applied at the original points $(\mathbf{k}_m, \mathbf{k}_{m+1})$. Let $\mathbf{h}^{a,b} \in \mathbb{R}^{d \times d}$ be the Hessian matrix between $(\mathbf{k}_a, \mathbf{k}_b)$. By using a modified Newton approach that maintains numerical stability, the solution for the optimal \mathbf{k}^* is derived:

$$\mathbf{k}^* = (\mathbf{h}^{m,m} + 2\mathbf{h}^{m,m+1} + \mathbf{h}^{m+1,m+1})^{-1} \left[\mathbf{h}^{m,m} \mathbf{k}_m + \mathbf{h}^{m,m+1} (\mathbf{k}_m + \mathbf{k}_{m+1}) + \mathbf{h}^{m+1,m+1} \mathbf{k}_{m+1} \right]. \quad (2)$$

In practice, the off-diagonal Hessian block $\mathbf{h}^{m,m+1}$ is ignored, and the diagonal elements are approximated using the Fisher Information Matrix (i.e., $\mathbf{h}^{ii} \approx (\nabla_i \mathcal{L})^2$). Under these simplifications, the optimal Key is constructed as a weighted aggregation:

$$\mathbf{k}^* \approx (\mathbf{h}^{m,m} + \mathbf{h}^{m+1,m+1})^{-1} (\mathbf{h}^{m,m} \mathbf{k}_m + \mathbf{h}^{m+1,m+1} \mathbf{k}_{m+1}). \quad (3)$$

For a merged adjacent pair $(m, m+1)$, the Value is combined by simple addition:

$$\mathbf{v}^* = \mathbf{v}_m + \mathbf{v}_{m+1}. \quad (4)$$

To optimize throughput, a chunk-based compression is implemented. Upon reaching the budget, AsymKV merges `chunk_size` adjacent pairs in parallel per new generated chunk, restoring the sequence length from `budget + chunk_size` back to the budget in a single step.

While current methods have made significant strides, they leave three key challenges unaddressed: (1) the theoretical explanation of KV asymmetry remains underexplored; (2) existing Hessian approximations overlook the off-diagonal couplings between Keys; and (3) a practical reliance on backpropagation persists, leading to non-negligible inference overhead. In this paper, we aim to address these challenges.

3.2. Theoretical Analysis of QKV Homogeneity and Heterogeneity

In this subsection, we establish a unified framework for QKV (dis)similarity by linking the spectral energy distribution of their projection weight matrices to their functional outcomes. Specifically, we show that projections that concentrate spectral energy induce adjacent homogeneity, whereas those with dispersed energy preserve heterogeneity.

Let $\mathbf{X} = \{\mathbf{x}_t\}_{t=1}^T$ denote the hidden-state sequence. For a specific attention head, the linear projection for the Query, Key, or Value can be generically represented as $\mathbf{y}_t = \mathbf{x}_t \mathbf{W}$, where $\mathbf{y} \in \{\mathbf{Q}, \mathbf{K}, \mathbf{V}\}$, $\mathbf{W} \in \{\mathbf{W}_Q, \mathbf{W}_K, \mathbf{W}_V\}$. Then, the cosine similarity between adjacent projected tokens $(\mathbf{x}_t, \mathbf{x}_{t+1})$ is defined as:

$$\cos(\mathbf{y}_t, \mathbf{y}_{t+1}) = \frac{(\mathbf{x}_t \mathbf{W})(\mathbf{x}_{t+1} \mathbf{W})^\top}{\|\mathbf{x}_t \mathbf{W}\|_2 \|\mathbf{x}_{t+1} \mathbf{W}\|_2}. \quad (5)$$

By defining the induced metric $\mathbf{M} \triangleq \mathbf{W} \mathbf{W}^\top$, we can reparameterize Eq. 5 within the input space:

$$\cos(\mathbf{y}_t, \mathbf{y}_{t+1}) = \frac{\mathbf{x}_t \mathbf{M} \mathbf{x}_{t+1}^\top}{\sqrt{\mathbf{x}_t \mathbf{M} \mathbf{x}_t^\top} \sqrt{\mathbf{x}_{t+1} \mathbf{M} \mathbf{x}_{t+1}^\top}}. \quad (6)$$

To elucidate the influence of the projection’s spectral properties, we apply Singular Value Decomposition (SVD) to the weight matrix $\mathbf{W} = \mathbf{U} \mathbf{\Sigma} \mathbf{V}^\top$, where $\mathbf{\Sigma} = \text{diag}(\sigma_1, \dots, \sigma_d)$. The induced metric \mathbf{M} thus admits the spectral decomposition $\mathbf{M} = \mathbf{U} \mathbf{\Sigma}^2 \mathbf{U}^\top = \sum_{i=1}^d \lambda_i \mathbf{u}_i \mathbf{u}_i^\top$, with $\lambda_i = \sigma_i^2$.

By projecting the input \mathbf{x}_t onto the modal coordinates spanned by the left singular vectors, denoted as $p_{t,i} \triangleq$

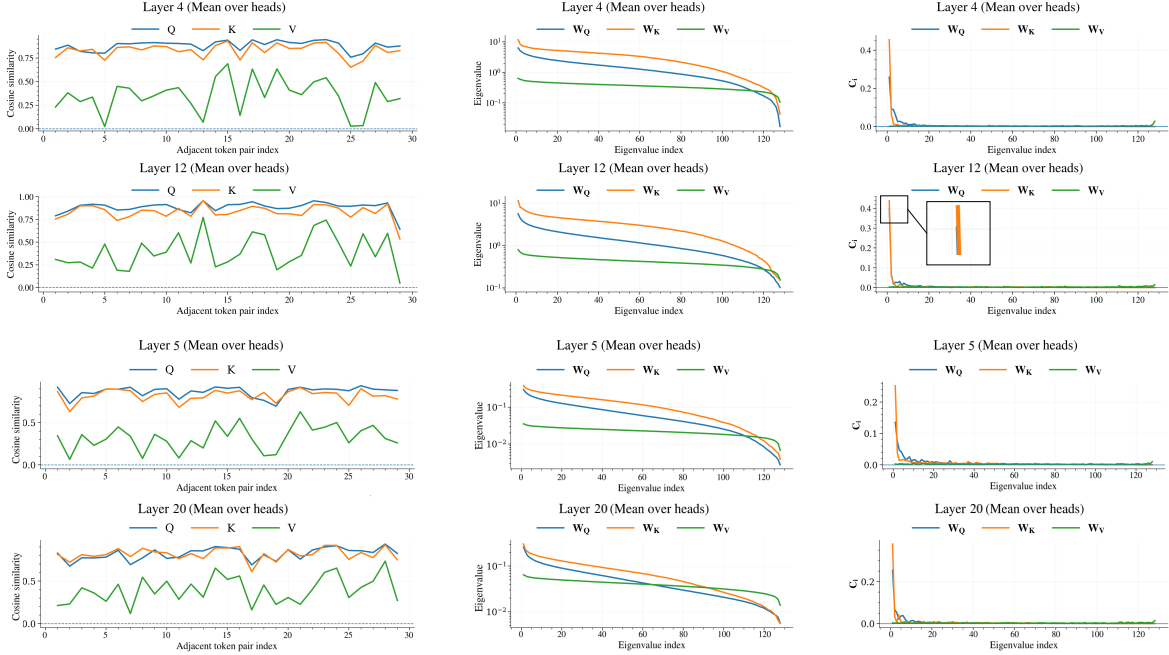


Figure 2. Layer-wise similarity and spectral analysis. **Left column:** Mean adjacent-token cosine similarity for Query (Q), Key (K), and Value (V), averaged over attention heads. **Middle column:** Eigenvalue distributions of the projection matrices \mathbf{W}_Q , \mathbf{W}_K , and \mathbf{W}_V , sorted in descending order. **Right column:** Mode-wise contribution coefficients c_i (Eq. 8), plotted according to the eigenvalue index. The first two rows show results from *Llama-3.1-8B-Instruct*, while the last two rows show results from *Mistral-7B-Instruct-v0.3*.

$\mathbf{x}_t \mathbf{u}_i$, the bilinear form can be expanded as $\mathbf{x}_t \mathbf{M} \mathbf{x}_{t+1}^\top = \sum_{i=1}^d \lambda_i p_{t,i} p_{t+1,i}$. Consequently, the cosine similarity admits an exact decomposition into the contributions of individual spectral modes:

$$\cos(\mathbf{y}_t, \mathbf{y}_{t+1}) = \frac{\sum_{i=1}^d \lambda_i p_{t,i} p_{t+1,i}}{\sqrt{\sum_{i=1}^d \lambda_i p_{t,i}^2} \sqrt{\sum_{i=1}^d \lambda_i p_{t+1,i}^2}}. \quad (7)$$

Furthermore, we define the relative contribution of the i -th spectral mode as:

$$c_i(\mathbf{y}_t, \mathbf{y}_{t+1}) \triangleq \frac{\lambda_i p_{t,i} p_{t+1,i}}{\sqrt{\sum_{j=1}^d \lambda_j p_{t,j}^2} \sqrt{\sum_{j=1}^d \lambda_j p_{t+1,j}^2}}, \quad (8)$$

which simplifies the similarity to a cumulative summation: $\cos(\mathbf{y}_t, \mathbf{y}_{t+1}) = \sum_{i=1}^d c_i(\mathbf{y}_t, \mathbf{y}_{t+1})$.

Since the spectral modes are ordered by decreasing eigenvalues λ_i , this formulation directly reveals that adjacent similarity is predominantly shaped by high-energy components, provided that the weight matrix exhibits a sharp spectral decay. As illustrated in Fig. 2¹, we empirically observe that \mathbf{W}_Q and \mathbf{W}_K projection weights possess a highly concentrated energy spectrum, inducing homogeneity by forcing adjacent embeddings into a shared subspace, while \mathbf{W}_V

projection possesses a relatively dispersed energy spectrum, resulting the heterogeneity.

This theoretical insight reveals an intriguing phenomenon within the attention mechanism. The Query and Key projections are inherently geared toward alignment. Their concentrated spectra effectively filter out high-frequency noise and project tokens into a shared semantic subspace, thereby inducing the stable similarity necessary for robust matching. In contrast, the Value projection is primarily responsible for information transmission. Its dispersed spectrum preserves the intrinsic heterogeneity, ensuring that the aggregated context remains expressive and information-rich rather than collapsing into a homogenized representation.

4. KVSlimmer

4.1. Exact Hessian Derivation for Key-Key Coupling

In this subsection, we formulate and derive the exact Hessian, explicitly capturing both the diagonal and off-diagonal coupling between adjacent keys, which prior art has overlooked.

Let \mathbf{q} be the Query, \mathbf{k}_i , \mathbf{v}_i be the Key and Value of the i -th token, respectively. The attention logit e_i , score α_i , and output o are defined as:

$$e_i = \frac{\mathbf{q} \mathbf{k}_i^\top}{\sqrt{d_k}}, \alpha_i = \frac{\exp e_i}{\sum_{t=1}^n \exp e_t}, \mathbf{o} = \sum_{t=1}^n \alpha_t \mathbf{v}_t, \quad (9)$$

¹More illustrations across different models are provided in Appendix. A.

where n is the sequence length. We denote the loss by \mathcal{L} and let $\mathbf{E} = \partial\mathcal{L}/\partial\mathbf{o}$ be the gradient of the loss with respect to the attention output.

We first derive the gradient $\mathbf{g}_i = \nabla_{\mathbf{k}_i}\mathcal{L}$. The Jacobian of the softmax is $\partial\alpha_j/\partial e_i = \alpha_j(\delta_{ji} - \alpha_i)$. Since e_i depends only on \mathbf{k}_i , we have:

$$\frac{\partial e_i}{\partial \mathbf{k}_i} = \frac{\mathbf{q}}{\sqrt{d_k}}, \quad \frac{\partial e_m}{\partial \mathbf{k}_i} = \mathbf{0} \text{ for } m \neq i. \quad (10)$$

Using the chain rule, the gradient of the output with respect to a key vector is:

$$\frac{\partial \mathbf{o}}{\partial \mathbf{k}_i} = \sum_{j=1}^n \mathbf{v}_j \frac{\partial \alpha_j}{\partial \mathbf{k}_i} = \frac{1}{\sqrt{d_k}} \alpha_i (\mathbf{v}_i - \mathbf{o}) \mathbf{q}^\top. \quad (11)$$

Therefore, the loss gradient with respect to \mathbf{k}_i is:

$$\mathbf{g}_i = \nabla_{\mathbf{k}_i}\mathcal{L} = \frac{\partial \mathcal{L}}{\partial \mathbf{o}} \frac{\partial \mathbf{o}}{\partial \mathbf{k}_i} = \frac{1}{\sqrt{d_k}} \alpha_i [\mathbf{E}^\top (\mathbf{v}_i - \mathbf{o})] \mathbf{q}. \quad (12)$$

We now compute the Hessian block $\mathbf{h}^{ij} = \partial \mathbf{g}_i / \partial \mathbf{k}_j^\top$, which captures the second-order interaction between the i -th and j -th Keys. Define $\mathbf{s}_i = \alpha_i (\mathbf{v}_i - \mathbf{o})$, so that $\mathbf{g}_i = \frac{1}{\sqrt{d_k}} (\mathbf{E}^\top \mathbf{s}_i) \mathbf{q}$, then:

$$\mathbf{h}^{ij} = \frac{1}{\sqrt{d_k}} \mathbf{q} \frac{\partial [\mathbf{E}^\top \mathbf{s}_i]}{\partial \mathbf{k}_j^\top}. \quad (13)$$

Since $e_j = \mathbf{q}^\top \mathbf{k}_j / \sqrt{d_k}$, we have $\partial e_j / \partial \mathbf{k}_j^\top = \mathbf{q}^\top / \sqrt{d_k}$. Applying the chain rule:

$$\frac{\partial \mathbf{s}_i}{\partial \mathbf{k}_j^\top} = \frac{\partial \mathbf{s}_i}{\partial e_j} \frac{\partial e_j}{\partial \mathbf{k}_j^\top} = \frac{1}{\sqrt{d_k}} \frac{\partial \mathbf{s}_i}{\partial e_j} \mathbf{q}^\top. \quad (14)$$

Substituting into Eq. 13 and using the linearity of \mathbf{E}^\top , we obtain:

$$\mathbf{h}^{ij} = \frac{1}{d_k} \left[\mathbf{E}^\top \frac{\partial \mathbf{s}_i}{\partial e_j} \right] \mathbf{q} \mathbf{q}^\top. \quad (15)$$

Thus, each Hessian block \mathbf{h}^{ij} is a rank-one matrix $\mathbf{q} \mathbf{q}^\top$ scaled by a scalar coefficient. To compute $\partial \mathbf{s}_i / \partial e_j$, expand $\mathbf{s}_i = \alpha_i \mathbf{v}_i - \alpha_i \mathbf{o}$:

$$\frac{\partial \mathbf{s}_i}{\partial e_j} = \frac{\partial \alpha_i}{\partial e_j} \mathbf{v}_i - \frac{\partial \alpha_i}{\partial e_j} \mathbf{o} - \alpha_i \frac{\partial \mathbf{o}}{\partial e_j}. \quad (16)$$

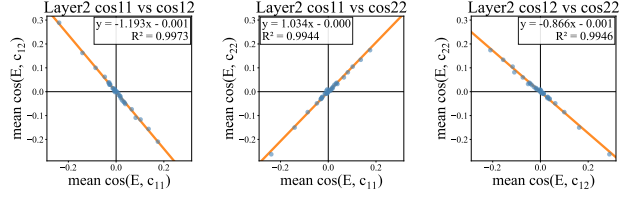
From the definition of \mathbf{o} and the softmax Jacobian, we have:

$$\frac{\partial \mathbf{o}}{\partial e_j} = \sum_{t=1}^n \mathbf{v}_t \frac{\partial \alpha_t}{\partial e_j} = \alpha_j (\mathbf{v}_j - \mathbf{o}). \quad (17)$$

Combining these results yields two distinct cases:

(1) Diagonal case ($j = i$), which captures the *self-sensitivity* of the i -th Key:

$$\frac{\partial \mathbf{s}_i}{\partial e_i} = \alpha_i (1 - 2\alpha_i) (\mathbf{v}_i - \mathbf{o}). \quad (18)$$



(a) $\cos(\mathbf{E}, \mathbf{c}_{11})$ vs. (b) $\cos(\mathbf{E}, \mathbf{c}_{11})$ vs. (c) $\cos(\mathbf{E}, \mathbf{c}_{12})$ vs. $\cos(\mathbf{E}, \mathbf{c}_{12})$ $\cos(\mathbf{E}, \mathbf{c}_{22})$ $\cos(\mathbf{E}, \mathbf{c}_{22})$

Figure 3. Head-level mean alignment relationships at Layer 2 of *Llama-3.1-8B-Instruct* on 2WikiMQA. Each point corresponds to one attention head, positioned by its global mean cosine alignment.

(2) Off-diagonal case ($j \neq i$), which captures the *coupling information* between i -th and j -th Keys:

$$\frac{\partial \mathbf{s}_i}{\partial e_j} = -\alpha_i \alpha_j (\mathbf{v}_i + \mathbf{v}_j - 2\mathbf{o}). \quad (19)$$

Thus, for any two adjacent Keys ($\mathbf{k}_m, \mathbf{k}_{m+1}$) targeted for merging, the precise Hessians are recovered as:

$$\mathbf{h}^{mm} = \frac{1}{d_k} [\mathbf{E}^\top \alpha_m (1 - 2\alpha_m) (\mathbf{v}_m - \mathbf{o})] \mathbf{q} \mathbf{q}^\top, \quad (20)$$

$$\mathbf{h}^{m+1, m+1} = \frac{1}{d_k} [\mathbf{E}^\top \alpha_{m+1} (1 - 2\alpha_{m+1}) (\mathbf{v}_{m+1} - \mathbf{o})] \mathbf{q} \mathbf{q}^\top, \quad (21)$$

$$\mathbf{h}^{m, m+1} = -\frac{1}{d_k} [\mathbf{E}^\top \alpha_m \alpha_{m+1} (\mathbf{v}_m + \mathbf{v}_{m+1} - 2\mathbf{o})] \mathbf{q} \mathbf{q}^\top, \quad (22)$$

with $\mathbf{h}^{m+1, m} = \mathbf{h}^{m, m+1}$.

4.2. Computation simplification

The exact Hessian blocks derived in Eqs. 20-22 enable precise computation of the optimal merged key in Eq. 2. However, this requires the loss gradient $\mathbf{E} = \partial\mathcal{L}/\partial\mathbf{o}$, necessitating expensive backpropagation. In this subsection, we eliminate gradient dependence, yielding a memory- and compute-efficient solution that preserves Hessian information precisely.

We begin by defining three vectors computed solely from the forward-pass:

$$\mathbf{c}_{11} = \alpha_m (1 - 2\alpha_m) (\mathbf{v}_m - \mathbf{o}), \quad (23)$$

$$\mathbf{c}_{22} = \alpha_{m+1} (1 - 2\alpha_{m+1}) (\mathbf{v}_{m+1} - \mathbf{o}), \quad (24)$$

$$\mathbf{c}_{12} = -\alpha_m \alpha_{m+1} (\mathbf{v}_m + \mathbf{v}_{m+1} - 2\mathbf{o}), \quad (25)$$

where $\mathbf{c}_{ij} \in \mathbb{R}^{d_v}$. The Hessian blocks \mathbf{h}^{ij} share a unified, rank-one form governed by scalar sensitivity $g_{ij} \triangleq \mathbf{E}^\top \mathbf{c}_{ij}$:

$$\mathbf{h}^{ij} = \frac{1}{d_k} g_{ij} \mathbf{q} \mathbf{q}^\top, \quad ij \in \{11, 12, 22\}. \quad (26)$$

Substituting Eq. 26 into Eq. 2 yields the linear system $\mathbf{M}\mathbf{k}^* = \mathbf{N}$, where

$$\mathbf{M} \triangleq \mathbf{h}^{11} + 2\mathbf{h}^{12} + \mathbf{h}^{22} = \frac{1}{d_k} \gamma \mathbf{q}\mathbf{q}^\top, \quad \gamma \triangleq g_{11} + 2g_{12} + g_{22}, \quad (27)$$

$$\mathbf{N} \triangleq \mathbf{h}^{11}\mathbf{k}_m + \mathbf{h}^{12}(\mathbf{k}_m + \mathbf{k}_{m+1}) + \mathbf{h}^{22}\mathbf{k}_{m+1} = \frac{1}{d_k} \mathbf{q}\mathbf{q}^\top \mathbf{b}, \quad (28)$$

with $\mathbf{b} \triangleq (g_{11} + g_{12})\mathbf{k}_m + (g_{12} + g_{22})\mathbf{k}_{m+1}$. Since $\mathbf{q}\mathbf{q}^\top$ is rank-one, a particular solution in $\text{span}\{\mathbf{q}\}$ is obtained via the Moore–Penrose pseudoinverse:

$$\begin{aligned} \mathbf{k}^* &= \mathbf{M}^+\mathbf{N} = \left(\frac{1}{d_k} \gamma \mathbf{q}\mathbf{q}^\top\right)^+ \left(\frac{1}{d_k} \mathbf{q}\mathbf{q}^\top \mathbf{b}\right) \\ &= \frac{1}{\gamma} (\mathbf{q}\mathbf{q}^\top)^+ (\mathbf{q}\mathbf{q}^\top) \mathbf{b} = \frac{1}{\gamma} \mathbf{P}_q \mathbf{b}, \end{aligned} \quad (29)$$

where $\mathbf{P}_q \triangleq (\mathbf{q}\mathbf{q}^\top)^+ (\mathbf{q}\mathbf{q}^\top)$ denotes the orthogonal projection onto $\text{span}\{\mathbf{q}\}$.

Crucially, the solution $\mathbf{k}^* = \frac{1}{\gamma} \mathbf{P}_q \mathbf{b}$ is confined to the one-dimensional subspace $\text{span}\{\mathbf{q}\}$. Therefore, we can equivalently express it within the original key space $\text{span}\{\mathbf{k}_m, \mathbf{k}_{m+1}\}$, which cancels the common factor $\mathbf{q}\mathbf{q}^\top$ and yields a pure weight form:

$$\mathbf{k}^* = w_m \mathbf{k}_m + w_{m+1} \mathbf{k}_{m+1}, \quad (30)$$

where $w_m = \frac{g_{11} + g_{12}}{g_{11} + 2g_{12} + g_{22}}$, $w_{m+1} = \frac{g_{12} + g_{22}}{g_{11} + 2g_{12} + g_{22}}$. Eq. 30 indicates that the optimal merging weights are determined solely by the relative magnitudes of the scalar sensitivity g_{ij} . The $g_{ij} = \mathbf{E}^\top \mathbf{c}_{ij}$ still depend on the gradient \mathbf{E} . Thus, we factor them into norm and angular components:

$$g_{ij} = \mathbf{E}^\top \mathbf{c}_{ij} = \|\mathbf{E}\|_2 \|\mathbf{c}_{ij}\|_2 \cos(\mathbf{E}, \mathbf{c}_{ij}), \quad ij \in \{11, 12, 22\}. \quad (31)$$

In regions where adjacent Keys are homogeneous, our empirical analysis in Fig. 3 reveals a consistent relation:

$$\cos(\mathbf{E}, \mathbf{c}_{11}) \approx \cos(\mathbf{E}, \mathbf{c}_{22}) \approx -\cos(\mathbf{E}, \mathbf{c}_{12}). \quad (32)$$

In Appendix. B and C, we provide more illustrations and a theoretical analysis for this relation, respectively. Plugging this relation into Eq. 30, the common factors cancel exactly and result in:

$$\begin{aligned} \mathbf{k}^* &= \left(\|\mathbf{c}_{11}\|_2 - 2\|\mathbf{c}_{12}\|_2 + \|\mathbf{c}_{22}\|_2 \right)^{-1} \\ &\quad \left[(\|\mathbf{c}_{11}\|_2 - \|\mathbf{c}_{12}\|_2) \mathbf{k}_m + (\|\mathbf{c}_{22}\|_2 - \|\mathbf{c}_{12}\|_2) \mathbf{k}_{m+1} \right]. \end{aligned} \quad (33)$$

Eq. 33 provides three key advantages: (1) it eliminates back-propagation and uses only forward-pass variables ($\alpha_i, \mathbf{v}_i, \mathbf{o}$); (2) it retains essential second-order Key–Key coupling interactions; (3) it involves only norm computations and linear combinations, adding negligible overhead.

5. Experiments

5.1. Experimental Setup

Baselines. We compare KVSlimmer against several categories of approaches: *context segmentation*: StreamingLLM (Xiao et al., 2024b) and LongCache (Liu et al., 2024b), *prompt compression*: LLMingua-2.0 (Pan et al., 2024), *KV cache compression*: H₂O (Zhang et al., 2023), *KV cache merge*: CaM (Zhang et al., 2024) and AsymKV (Cui & Xu, 2025).

Base Models. To demonstrate the generality of KVSlimmer, we conduct evaluations across a diverse set of model architectures, including Llama3.1-8B-Instruct (Dubey et al., 2024), Mistral-7B-Instruct-v0.3 (Jiang et al., 2023) and Qwen2-1.5B-Instruct (Yang et al., 2024).

Implementation Details. Unless otherwise specified, we set the compression context budget to 2048 tokens and the compression granularity chunk_size to 512. All baseline methods are evaluated under identical configurations to ensure fair comparison. For H₂O, we follow the original setup by allocating a recent-token budget of 2048 and a heavy-token budget of 512. Following Attention Sink (Xiao et al., 2024b), the initial 32 tokens are always preserved. All experiments are conducted on one NVIDIA A100 GPU with 80GB of memory.

5.2. Long Context Performance Evaluation

We evaluate KVSlimmer’s effectiveness on LongBench (Bai et al., 2024), a comprehensive long-context benchmark, containing 16 English tasks from a wide range of categories.

Results. As summarized in Table 1, KVSlimmer achieves the SOTA performance on LongBench, demonstrating consistent advantages across various model architectures and task categories. Specifically, on Llama3.1-8B-Instruct, KVSlimmer reaches an average score of 44.04, surpassing the previous SOTA, AsymKV, by a margin of 0.92. Notably, the gains are particularly pronounced in long-context–sensitive tasks. For instance, it yields improvements of 0.82, 0.68, and 5.13 on Single-Doc, Multi-Doc, and Synthetic tasks, respectively. Similarly, on Mistral-7B-Instruct-v0.3, KVSlimmer obtains the highest average score of 41.28, outperforming AsymKV by 0.40 and setting new benchmarks in Few-shot, Code, and Synthetic categories. Even on the more compact Qwen2-1.5B-Instruct model, KVSlimmer maintains its lead with an average score of 32.45. This underscores its capability to effectively preserve critical information during KV merging, even when constrained by limited model capacity.

Extreme Long-Context Compression. We evaluate KVSlimmer on LongBenchV2 (Bai et al., 2025), which comprises contexts ranging from 8K to 2M tokens across six

KVSlimmer: Theoretical Insights and Practical Optimizations for Asymmetric KV Merging

Table 1. Performance on LongBench. KVSlimmer outperforms its baselines on most settings.

	Single-Doc	Multi-Doc	Sum	Few-shot	Synthetic	Code	Avg.
Llama3.1-8B-Instruct							
Full Context	43.73	44.49	29.12	69.36	53.56	50.95	48.07
StreamingLLM	28.15	27.19	25.15	63.17	16.33	52.15	35.50
LongCache	28.98	27.84	25.35	64.73	19.68	51.61	36.46
H ₂ O	33.30	34.43	26.60	66.23	14.75	52.65	38.53
LLMLingua-2	32.02	32.24	24.99	27.87	17.67	50.07	30.43
CaM	32.14	32.63	24.91	63.09	16.77	52.13	37.26
AsymKV	39.42	38.93	27.30	65.66	39.39	48.57	43.12
KVSlimmer	40.24	39.61	27.19	65.00	44.52	49.73	44.04
Mistral-7B-Instruct-v0.3							
Full Context	38.74	38.29	29.04	70.70	51.00	53.05	46.15
StreamingLLM	24.80	22.14	25.18	66.49	15.14	52.10	34.39
LongCache	26.05	22.31	25.44	66.21	14.93	51.03	34.50
H ₂ O	29.66	28.22	26.32	67.78	14.83	51.63	36.80
LLMLingua-2	28.12	28.62	25.75	45.85	16.00	46.50	31.88
CaM	26.15	29.06	26.81	66.16	20.96	51.40	36.83
AsymKV	33.71	32.81	27.04	67.21	34.56	51.33	40.88
KVSlimmer	33.42	32.62	26.83	67.86	36.78	52.34	41.28
Qwen2-1.5B-Instruct							
Full Context	30.03	28.68	26.16	66.68	5.50	41.49	34.29
StreamingLLM	21.62	19.70	21.95	61.68	3.50	41.38	29.04
LongCache	22.22	27.31	16.28	56.65	5.25	41.21	28.76
H ₂ O	26.50	29.22	13.77	51.92	4.25	39.02	28.17
LLMLingua-2	21.83	20.94	15.67	57.31	4.00	38.91	27.07
CaM	24.76	19.46	16.38	58.19	3.75	36.39	27.29
AsymKV	26.14	27.70	23.33	62.99	4.75	40.89	31.98
KVSlimmer	26.54	29.54	23.90	61.54	5.50	41.84	32.45

task categories. The results, obtained using Llama3.1-8B-Instruct with a cache size of 8192, are reported in Table 2. Notably, KVSlimmer outperforms SOTA methods across Easy, Short, and Long categories, resulting in the best overall performance. These results demonstrate KVSlimmer’s robustness and effectiveness in handling extremely long contexts under constrained cache budgets.

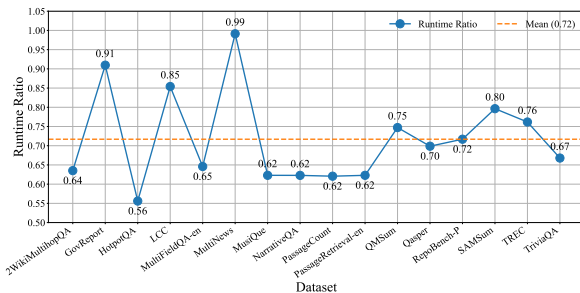


Figure 4. Relative runtime of KVSlimmer compared to AsymKV across LongBench datasets.

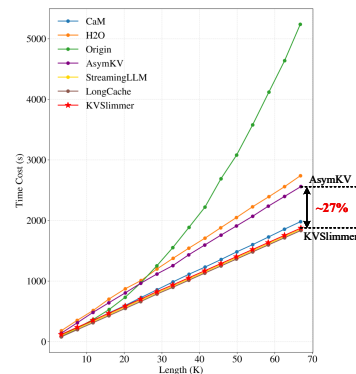


Figure 5. Inference efficiency of decoder stage.

Table 2. Performance on LongBenchV2.

Model	Overall	Easy	Hard	Short	Medium	Long
Full Context	30.02	30.73	29.58	35.00	27.91	25.93
StreamingLLM	27.04	27.60	26.69	32.78	23.26	25.00
LongCache	28.43	28.13	28.62	32.78	25.58	26.85
H ₂ O	28.23	28.12	28.29	31.67	26.98	25.00
CaM	28.23	28.64	27.97	31.67	26.98	25.00
AsymKV	30.02	30.23	29.90	32.78	27.44	28.85
KVSlimmer	30.22	32.81	28.62	36.11	25.12	30.56

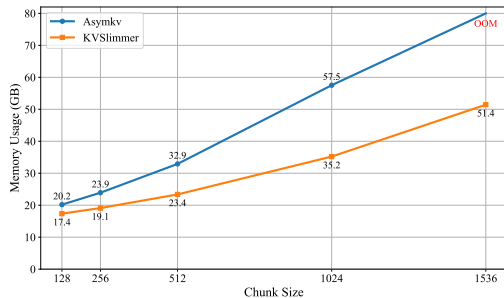


Figure 6. Peak GPU memory of KVSlimmer and AsymKV across different chunk sizes.

5.3. Runtime/Memory Efficiency

Fig. 4 illustrates the relative runtime of KVSlimmer compared with AsymKV across LongBench datasets. While KVSlimmer performs similarly to AsymKV on shorter tasks (e.g., GovReport and MultiNews), it demonstrates a substantial advantage in time efficiency as sequence length increases. For instance, KVSlimmer achieves a 44% reduction in runtime on long-context HotpotQA, and a 38% reduction on MusiQue, NarrativeQA, PassageCount, and PassageRetrieval-en. Overall, KVSlimmer consistently reduces inference latency by an average of 28%, highlighting its superior computational efficiency. Fig. 5 compares the runtime of generating long-context sequences. As can be seen, thanks to the minimal KV cache operations, KVSlimmer reduces the time overhead much more significantly than AsymKV, and even yields comparable latency to context-segmentation approaches (e.g., StreamingLLM and LongCache). These results demonstrate that KVSlimmer strikes a better balance between efficiency and effectiveness.

Fig. 6 compares the peak GPU memory usage of KVSlimmer and AsymKV across various chunk sizes, averaged over all 16 LongBench tasks. While memory consumption for both methods scales with chunk size, KVSlimmer consistently maintains a significantly lower memory footprint. Notably, this efficiency gap widens as the chunk size grows. KVSlimmer achieves memory reductions of 29% and 39% at chunk sizes of 512 and 1024, respectively. These results demonstrate that KVSlimmer effectively mitigates memory pressure induced by large chunks, enabling more aggressive

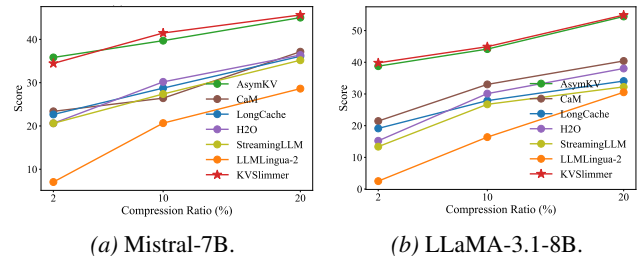


Figure 7. Results on different compression ratios.

chunking strategies and more stable long-context inference within constrained GPU memory budgets.

5.4. Compression Rate Analysis

To systematically compare the context compression capabilities of KVSlimmer and AsymKV, we analyze their performance across various compression ratios on the LongBench HotpotQA (Yang et al., 2018) task. We define the compression ratio as the number of retained tokens relative to the original sequence length. As illustrated in Fig. 7, KVSlimmer consistently achieves slightly superior performance compared to AsymKV on average. More importantly, KVSlimmer incurs significantly lower computational and memory overhead. For instance, at a 10% compression ratio, it reduces latency and memory usage by $\sim 20\%$ and $\sim 27\%$, respectively.

6. Discussion

Despite its theoretical and empirical advantages, KVSlimmer has several limitations that invite future exploration. First, our spectral analysis and merging strategy primarily focus on local token sequences. Exploring non-local or global merging could potentially yield even higher compression ratios by capturing long-range dependencies. Second, although KVSlimmer is gradient-free and time-efficient, the current implementation employs a uniform compression ratio across all layers. Developing adaptive compression strategies that dynamically adjust the merging intensity based on the specific importance of each layer represents a promising direction for future research.

7. Conclusion

In this paper, we introduced KVSlimmer, a theoretically grounded and computationally efficient framework for asymmetric KV cache compression. By establishing a unified spectral analysis framework, we first unraveled the theoretical origins of QKV asymmetry in LLMs, demonstrating how the spectral energy distribution of projection weights dictates homogeneity and heterogeneity. Then, we introduce KVSlimmer, which derives a mathematically exact Hessian formulation that captures the off-diagonal coupling between adjacent Keys and achieves a gradient-free, closed-form solution that relies solely on forward-pass variables, reducing the memory and time overhead by a large margin. Extensive experiments on various LLMs and benchmarks validate that KVSlimmer significantly reduces memory and latency while maintaining, or even enhancing, model performance on long-context tasks.

Impact Statement

This paper presents work whose goal is to advance the field of Machine Learning. There are many potential societal consequences of our work, none of which we feel must be specifically highlighted here.

References

- Ainslie, J., Ontañón, S., Alberti, C., Cvicek, V., Fisher, Z., Pham, P., Ravula, A., Sanghai, S., Wang, Q., and Yang, L. ETC: Encoding long and structured inputs in transformers. In Webber, B., Cohn, T., He, Y., and Liu, Y. (eds.), *Proceedings of the 2020 Conference on Empirical Methods in Natural Language Processing (EMNLP)*, pp. 268–284, Online, November 2020. Association for Computational Linguistics. doi: 10.18653/v1/2020.emnlp-main.19.
- An, C., Huang, F., Zhang, J., Gong, S., Qiu, X., Zhou, C., and Kong, L. Training-free long-context scaling of large language models. *CoRR*, abs/2402.17463, 2024.
- Bai, Y., Lv, X., Zhang, J., Lyu, H., Tang, J., Huang, Z., Du, Z., Liu, X., Zeng, A., Hou, L., Dong, Y., Tang, J., and Li, J. LongBench: A bilingual, multitask benchmark for long context understanding. In *Proceedings of the 62nd Annual Meeting of the Association for Computational Linguistics (Volume 1: Long Papers)*, pp. 3119–3137, Bangkok, Thailand, August 2024. Association for Computational Linguistics. doi: 10.18653/v1/2024.acl-long.172.
- Bai, Y., Tu, S., Zhang, J., Peng, H., Wang, X., Lv, X., Cao, S., Xu, J., Hou, L., Dong, Y., et al. Longbench v2: Towards deeper understanding and reasoning on realistic long-context multitasks. In *Proceedings of the 63rd Annual Meeting of the Association for Computational Linguistics (Volume 1: Long Papers)*, pp. 3639–3664, 2025.
- Beltagy, I., Peters, M. E., and Cohan, A. Longformer: The long-document transformer. *CoRR*, abs/2004.05150, 2020.
- Brandon, W., Mishra, M., Nrusimha, A., Panda, R., and Ragan-Kelley, J. Reducing transformer key-value cache size with cross-layer attention. In *The Thirty-eighth Annual Conference on Neural Information Processing Systems*, 2024.
- Bulatov, A., Kuratov, Y., and Burtsev, M. S. Recurrent memory transformer. In *Proceedings of the 36th International Conference on Neural Information Processing Systems, NIPS '22*, Red Hook, NY, USA, 2022. Curran Associates Inc. ISBN 9781713871088.
- Cai, Z., Zhang, Y., Gao, B., Liu, Y., Li, Y., Liu, T., Lu, K., Xiong, W., Dong, Y., Hu, J., and Xiao, W. PyramidKV: Dynamic KV cache compression based on pyramidal information funneling. In *Second Conference on Language Modeling*, 2025.
- Chang, C.-C., Lin, C.-Y., Akhauri, Y., Lin, W.-C., Wu, K.-C., Ceze, L., and Abdelfattah, M. S. xkv: Cross-layer svd for kv-cache compression, 2025.
- Chitty-Venkata, K. T., Ye, J., Sun, X.-H., Kougkas, A., Emani, M., Vishwanath, V., and Nicolae, B. Pagedevic-tion: Structured block-wise kv cache pruning for efficient large language model inference, 2025.
- Cui, W. and Xu, M. Homogeneous keys, heterogeneous values: Exploiting local KV cache asymmetry for long-context LLMs. In *The Thirty-ninth Annual Conference on Neural Information Processing Systems*, 2025.
- Dai, Z., Yang, Z., Yang, Y., Carbonell, J., Le, Q., and Salakhutdinov, R. Transformer-XL: Attentive language models beyond a fixed-length context. In Korhonen, A., Traum, D., and Màrquez, L. (eds.), *Proceedings of the 57th Annual Meeting of the Association for Computational Linguistics*, pp. 2978–2988, Florence, Italy, July 2019. Association for Computational Linguistics. doi: 10.18653/v1/P19-1285.
- Dao, T., Fu, D., Ermon, S., Rudra, A., and Ré, C. Flashat-tention: Fast and memory-efficient exact attention with io-awareness. In Koyejo, S., Mohamed, S., Agarwal, A., Belgrave, D., Cho, K., and Oh, A. (eds.), *Advances in Neural Information Processing Systems*, volume 35, pp. 16344–16359. Curran Associates, Inc., 2022.
- Dubey, A., Jauhri, A., Pandey, A., Kadian, A., Al-Dahle, A., Letman, A., Mathur, A., Schelten, A., Yang, A., Fan, A., et al. The llama 3 herd of models. *arXiv preprint arXiv:2407.21783*, 2024.

- Feng, S., Liu, Y., Li, H., Chen, X., Shen, S., Du, K., Gu, Z., Zhang, R., Huang, Y., Cheng, Y., Yao, J., Zhang, Q., Ananthanarayanan, G., and Jiang, J. Evicpress: Joint kv-cache compression and eviction for efficient llm serving, 2025a.
- Feng, Y., Guo, H., Lv, J., Zhou, S. K., and Xie, X. Taming the fragility of kv cache eviction in llm inference, 2025b.
- Fu, Y., Cai, Z., Asi, A., Xiong, W., Dong, Y., and Xiao, W. Not all heads matter: A head-level KV cache compression method with integrated retrieval and reasoning. In *The Thirteenth International Conference on Learning Representations*, 2025.
- Ge, S., Zhang, Y., Liu, L., Zhang, M., Han, J., and Gao, J. Model tells you what to discard: Adaptive KV cache compression for LLMs. In *Workshop on Advancing Neural Network Training: Computational Efficiency, Scalability, and Resource Optimization (WANT@NeurIPS 2023)*, 2023.
- Ge, S., Zhang, Y., Liu, L., Zhang, M., Han, J., and Gao, J. Model tells you what to discard: Adaptive KV cache compression for LLMs. In *The Twelfth International Conference on Learning Representations*, 2024.
- Gu, Y., Jiang, Z., Jin, J., Guo, K., Zhang, Z., and Xu, X. Ahakv: Adaptive holistic attention-driven kv cache eviction for efficient inference of large language models, 2025a.
- Gu, Y., Liang, X., Zhao, J., and Diao, E. Obcache: Optimal brain kv cache pruning for efficient long-context llm inference, 2025b.
- Huang, Y., Xu, J., Lai, J., Jiang, Z., Chen, T., Li, Z., Yao, Y., Ma, X., Yang, L., Chen, H., Li, S., and Zhao, P. Advancing transformer architecture in long-context large language models: A comprehensive survey, 2024. URL <https://arxiv.org/abs/2311.12351>.
- Jiang, A. Q., Sablayrolles, A., Mensch, A., Bamford, C., Chaplot, D. S., de las Casas, D., Bressand, F., Lengyel, G., Lample, G., Saulnier, L., Lavaud, L. R., Lachaux, M.-A., Stock, P., Scao, T. L., Lavril, T., Wang, T., Lacroix, T., and Sayed, W. E. Mistral 7b, 2023.
- Keles, F. D., Wijewardena, P. M., and Hegde, C. On the computational complexity of self-attention. *CoRR*, abs/2209.04881, 2022.
- Kim, M., Kundu, A., Kim, H.-B., Dixit, R., and Cho, M. Epicache: Episodic kv cache management for long conversational question answering, 2025.
- Łańcucki, A., Staniszewski, K., Nawrot, P., and Ponti, E. Inference-time hyper-scaling with KV cache compression. In *The Thirty-ninth Annual Conference on Neural Information Processing Systems*, 2025.
- Li, K., Xiong, Y., Jiang, Z., Zhou, Y., Wang, Z., Lv, C., and Zhang, S. Flowmm: Cross-modal information flow guided kv cache merging for efficient multimodal context inference, 2025a.
- Li, Y., Huang, Y., Yang, B., Venkitesh, B., Locatelli, A., Ye, H., Cai, T., Lewis, P., and Chen, D. Snapkv: Llm knows what you are looking for before generation. In *Advances in Neural Information Processing Systems 37*, NIPS '24, Red Hook, NY, USA, 2024. Curran Associates Inc. ISBN 9798331314385.
- Li, Y., Li, Y., Meng, Y., Ma, X., Geng, Z., Xia, S., and Wang, Z. Ems: Adaptive evict-then-merge strategy for head-wise kv cache compression based on global-local importance, 2025b.
- Liu, A., Liu, J., Pan, Z., He, Y., Haffari, G., and Zhuang, B. Minicache: KV cache compression in depth dimension for large language models. In *The Thirty-eighth Annual Conference on Neural Information Processing Systems*, 2024a.
- Liu, X., Guo, Q., Song, Y., Liu, Z., Lv, K., Yan, H., Li, L., Liu, Q., and Qiu, X. Farewell to length extrapolation, a training-free infinite context with finite attention scope. *arXiv preprint arXiv:2407.15176*, 2024b.
- Liu, X., Li, R., Huang, M., Liu, Z., Song, Y., Guo, Q., He, S., Wang, Q., Li, L., Liu, Q., He, Z., Zhou, Y., Huang, X., and Qiu, X. Thus spake long-context large language model, 2025a. URL <https://arxiv.org/abs/2502.17129>.
- Liu, X., Wang, X., Liu, P., and Tang, G. Zsmerge: Zero-shot kv cache compression for memory-efficient long-context llms, 2025b.
- Liu, Y., Yu, J., Xu, Y., Li, Z., and Zhu, Q. A survey on transformer context extension: Approaches and evaluation, 2025c. URL <https://arxiv.org/abs/2503.13299>.
- Liu, Z., Desai, A., Liao, F., Wang, W., Xie, V., Xu, Z., Kyriillidis, A., and Shrivastava, A. Scissorhands: Exploiting the persistence of importance hypothesis for llm kv cache compression at test time. In Oh, A., Naumann, T., Globerson, A., Saenko, K., Hardt, M., and Levine, S. (eds.), *Advances in Neural Information Processing Systems*, volume 36, pp. 52342–52364. Curran Associates, Inc., 2023a.

- Liu, Z., Desai, A., Liao, F., Wang, W., Xie, V., Xu, Z., Kyriillidis, A., and Shrivastava, A. Scissorhands: Exploiting the persistence of importance hypothesis for LLM KV cache compression at test time. In *Thirty-seventh Conference on Neural Information Processing Systems*, 2023b.
- Nawrot, P., Łańcucki, A., Chochowski, M., Tarjan, D., and Ponti, E. M. Dynamic memory compression: retrofitting llms for accelerated inference. In *Proceedings of the 41st International Conference on Machine Learning*, ICML'24. JMLR.org, 2024.
- Pan, Z., Wu, Q., Jiang, H., Xia, M., Luo, X., Zhang, J., Lin, Q., Ruhle, V., Yang, Y., Lin, C.-Y., Zhao, H. V., Qiu, L., and Zhang, D. LLMingua-2: Data distillation for efficient and faithful task-agnostic prompt compression. In Ku, L.-W., Martins, A., and Srikumar, V. (eds.), *Findings of the Association for Computational Linguistics ACL 2024*, pp. 963–981, Bangkok, Thailand and virtual meeting, August 2024. Association for Computational Linguistics.
- Rae, J. W., Potapenko, A., Jayakumar, S. M., Hillier, C., and Lillicrap, T. P. Compressive transformers for long-range sequence modelling. In *International Conference on Learning Representations*, 2020.
- Tian, Y., Wang, Z., Peng, Y., Yuan, A., Wang, Z., Yi, B., Liu, X., Cui, Y., and Yang, T. Keepkv: Achieving periodic lossless kv cache compression for efficient llm inference, 2025.
- Wan, Z., Wu, X., Zhang, Y., Xin, Y., Tao, C., Zhu, Z., Wang, X., Luo, S., Xiong, J., Wang, L., and Zhang, M. D₂O : Dynamic discriminative operations for efficient long-context inference of large language models. In *The Thirteenth International Conference on Learning Representations*, 2025.
- Wang, X., Salmani, M., Omidi, P., Ren, X., Rezagholizadeh, M., and Eshaghi, A. Beyond the limits: a survey of techniques to extend the context length in large language models. In *Proceedings of the Thirty-Third International Joint Conference on Artificial Intelligence, IJCAI '24*, 2024a. ISBN 978-1-956792-04-1. doi: 10.24963/ijcai.2024/917.
- Wang, Y., Ji, S., Liu, Y., Xu, Y., Xu, Y., Zhu, Q., and Che, W. Lookahead q-cache: Achieving more consistent kv cache eviction via pseudo query, 2025a.
- Wang, Z., Jin, B., Yu, Z., and Zhang, M. Model tells you where to merge: Adaptive kv cache merging for llms on long-context tasks, 2024b.
- Wang, Z., Jin, B., Chang, Y., Yu, Z., and Zhang, M. Model tells you where to merge: Adaptive KV cache merging for LLMs on long-context tasks, 2025b.
- Wu, W., Pan, Z., Fu, K., Wang, C., Chen, L., Bai, Y., Wang, T., Wang, Z., and Xiong, H. TokenSelect: Efficient long-context inference and length extrapolation for LLMs via dynamic token-level KV cache selection. In Christodoulopoulos, C., Chakraborty, T., Rose, C., and Peng, V. (eds.), *Proceedings of the 2025 Conference on Empirical Methods in Natural Language Processing*, pp. 21264–21281, Suzhou, China, November 2025. Association for Computational Linguistics. ISBN 979-8-89176-332-6. doi: 10.18653/v1/2025.emnlp-main.1079.
- Xiao, C., Zhang, P., Han, X., Xiao, G., Lin, Y., Zhang, Z., Liu, Z., and Sun, M. Inllm: training-free long-context extrapolation for llms with an efficient context memory. In *Advances in Neural Information Processing Systems 37*, NIPS '24, Red Hook, NY, USA, 2024a. Curran Associates Inc. ISBN 9798331314385.
- Xiao, G., Tian, Y., Chen, B., Han, S., and Lewis, M. Efficient streaming language models with attention sinks. In *The Twelfth International Conference on Learning Representations*, 2024b.
- Yang, A., Yang, B., Hui, B., Zheng, B., Yu, B., Zhou, C., Li, C., Li, C., Liu, D., Huang, F., Dong, G., Wei, H., Lin, H., Tang, J., Wang, J., Yang, J., Tu, J., Zhang, J., Ma, J., Yang, J., Xu, J., Zhou, J., Bai, J., He, J., Lin, J., Dang, K., Lu, K., Chen, K., Yang, K., Li, M., Xue, M., Ni, N., Zhang, P., Wang, P., Peng, R., Men, R., Gao, R., Lin, R., Wang, S., Bai, S., Tan, S., Zhu, T., Li, T., Liu, T., Ge, W., Deng, X., Zhou, X., Ren, X., Zhang, X., Wei, X., Ren, X., Liu, X., Fan, Y., Yao, Y., Zhang, Y., Wan, Y., Chu, Y., Liu, Y., Cui, Z., Zhang, Z., Guo, Z., and Fan, Z. Qwen2 technical report, 2024.
- Yang, Z., Qi, P., Zhang, S., Bengio, Y., Cohen, W., Salakhutdinov, R., and Manning, C. D. Hotpotqa: A dataset for diverse, explainable multi-hop question answering. In *Proceedings of the 2018 Conference on Empirical Methods in Natural Language Processing*, pp. 2369–2380, 2018.
- Yuan, J., He, Z., Bai, H., Leng, J., and Jiang, B. Weightedkv: Attention scores weighted key-value cache merging for large language models, 2025.
- Zaheer, M., Guruganesh, G., Dubey, K. A., Ainslie, J., Alberti, C., Ontañón, S., Pham, P., Ravula, A., Wang, Q., Yang, L., and Ahmed, A. Big bird: Transformers for longer sequences. In *NeurIPS*, 2020.
- Zhang, Y., Du, Y., Luo, G., Zhong, Y., Zhang, Z., Liu, S., and Ji, R. Cam: Cache merging for memory-efficient

LLMs inference. In *Forty-first International Conference on Machine Learning*, 2024.

Zhang, Z., Sheng, Y., Zhou, T., Chen, T., Zheng, L., Cai, R., Song, Z., Tian, Y., Ré, C., Barrett, C., Wang, Z. A., and Chen, B. H2o: Heavy-hitter oracle for efficient generative inference of large language models. In Oh, A., Naumann, T., Globerson, A., Saenko, K., Hardt, M., and Levine, S. (eds.), *Advances in Neural Information Processing Systems*, volume 36, pp. 34661–34710. Curran Associates, Inc., 2023.

Zhu, S., Ye, J., Jiang, W., Xue, S., Zhang, Q., Wu, Y., and Li, J. CoCA: Fusing position embedding with collinear constrained attention in transformers for long context window extending. In Ku, L.-W., Martins, A., and Srikumar, V. (eds.), *Proceedings of the 62nd Annual Meeting of the Association for Computational Linguistics (Volume 1: Long Papers)*, pp. 4247–4262, Bangkok, Thailand, August 2024. Association for Computational Linguistics. doi: 10.18653/v1/2024.acl-long.233.

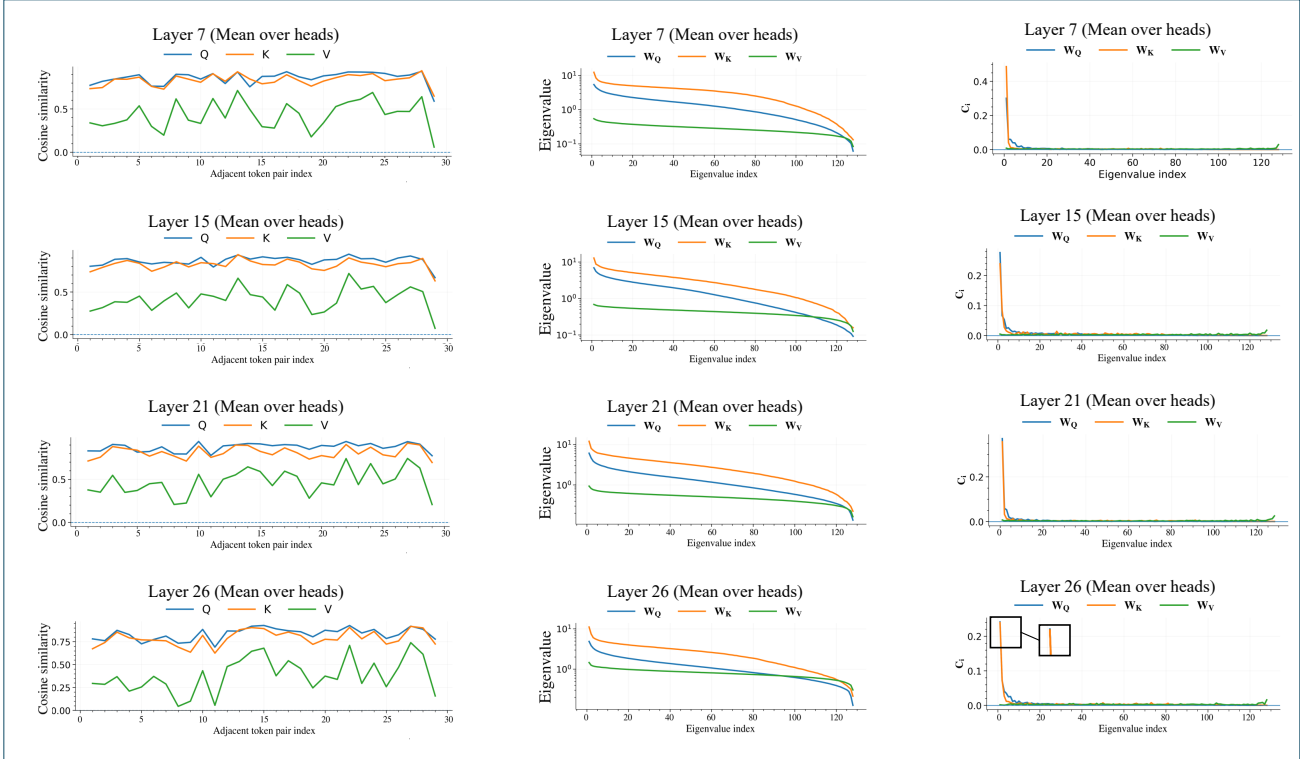


Figure 8. Layer-wise QKV similarity and spectral analysis for *Llama-3.1-8B-Instruct*. Left column: Mean adjacent-token cosine similarity for Query (Q), Key (K), and Value (V), averaged over attention heads. Middle column: Eigenvalue distributions of the projection matrices \mathbf{W}_Q , \mathbf{W}_K , and \mathbf{W}_V , sorted in descending order. Right column: Mode-wise contribution coefficients c_i (Eq. 8), plotted according to the eigenvalue index.

A. More Illustrations of Layer-wise QKV Similarity and Spectral Analysis

In Fig. 8 and Fig. 9, we provide more layer-wise QKV similarity and spectral analysis across different models.

B. Head-Level Alignment Illustrations

In Fig. 10, Fig. 11, Fig. 12, Fig. 13, Fig. 14, we provide more head-level alignment illustrations.

C. Theoretical Analysis of Eq. 32

For a fixed attention head and a query position q , the head output is

$$\mathbf{o} = \sum_i \alpha_i \mathbf{v}_i, \quad \alpha_i = \text{softmax}(z_i), \quad z_i = \frac{1}{\sqrt{d_k}} \mathbf{q}^\top \mathbf{k}_i. \quad (34)$$

Define the gradient of the loss with respect to the head output as

$$\mathbf{E} \triangleq \frac{\partial L}{\partial \mathbf{o}}. \quad (35)$$

During training, the model is optimized by minimizing the empirical risk

$$\min_{\theta} \frac{1}{N} \sum_{n=1}^N L^{(n)}(\theta). \quad (36)$$

Importantly, \mathbf{E} is not generated in response to any particular local residual $\mathbf{v}_i - \mathbf{o}$. Rather, it is the head-level first-order descent signal induced by empirical risk minimization. Concretely, \mathbf{E} is determined by the downstream network and the final

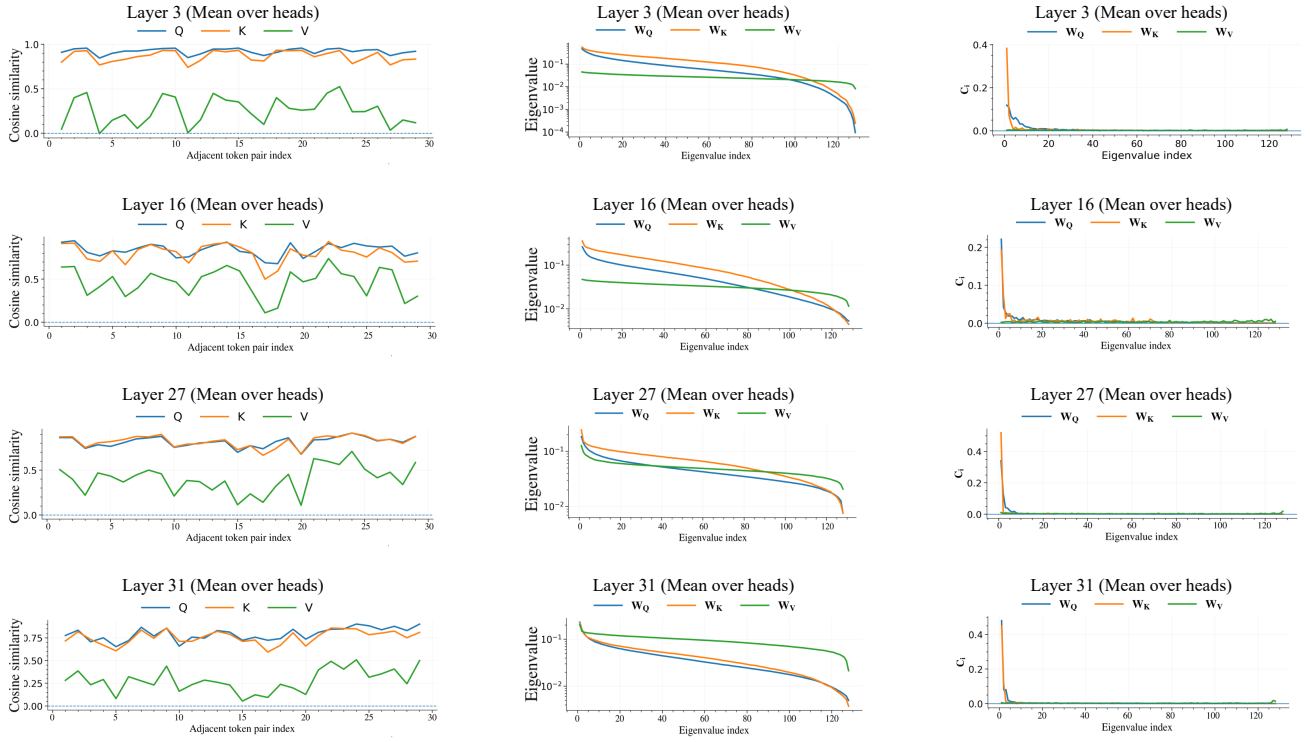


Figure 9. Layer-wise QKV similarity and spectral analysis for *Mistral-7B-Instruct-v0.3*. Left column: Mean adjacent-token cosine similarity for Query (Q), Key (K), and Value (V), averaged over attention heads. Middle column: Eigenvalue distributions of the projection matrices \mathbf{W}_Q , \mathbf{W}_K , and \mathbf{W}_V , sorted in descending order. Right column: Mode-wise contribution coefficients c_i (Eq. 8), plotted according to the eigenvalue index.

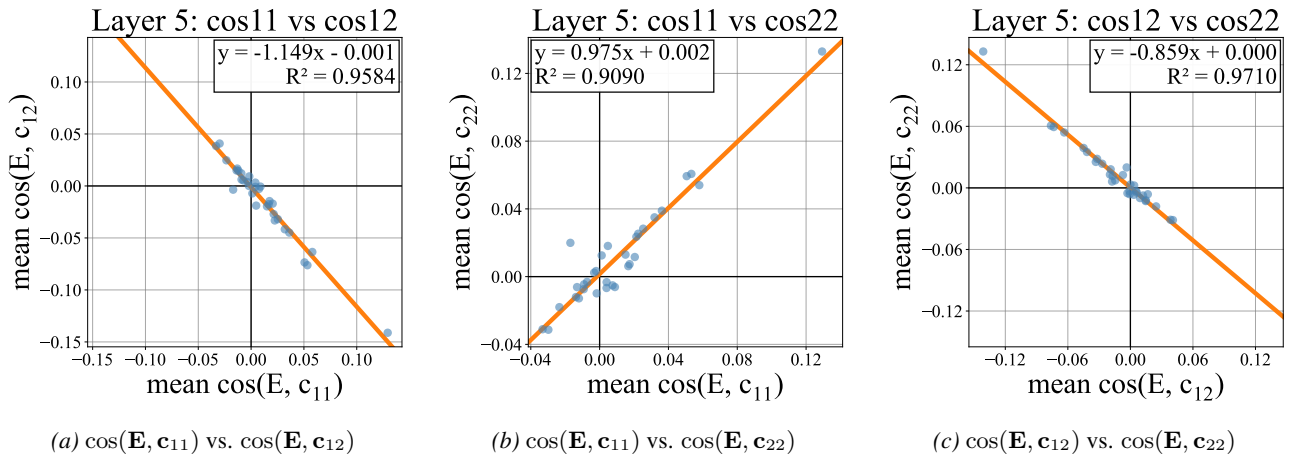


Figure 10. Head-level mean alignment relationships at Layer 5 of *Llama-3.1-8B-Instruct* on 2WikiMQA. Each point corresponds to one attention head, positioned by its global mean cosine alignment.

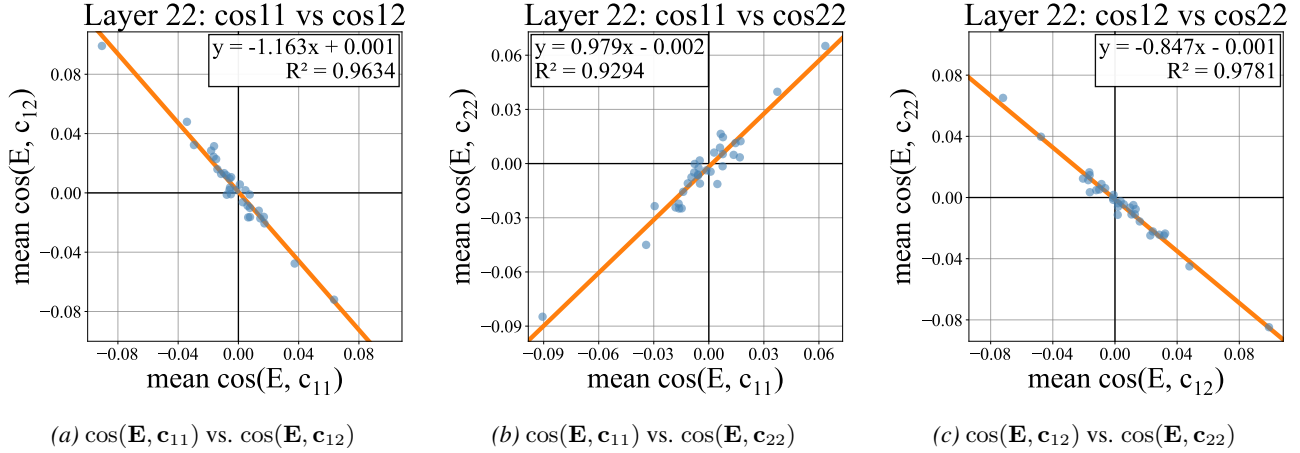


Figure 11. Head-level mean alignment relationships at Layer 22 of *Llama-3.1-8B-Instruct* on 2WikiMQA. Each point corresponds to one attention head, positioned by its global mean cosine alignment.

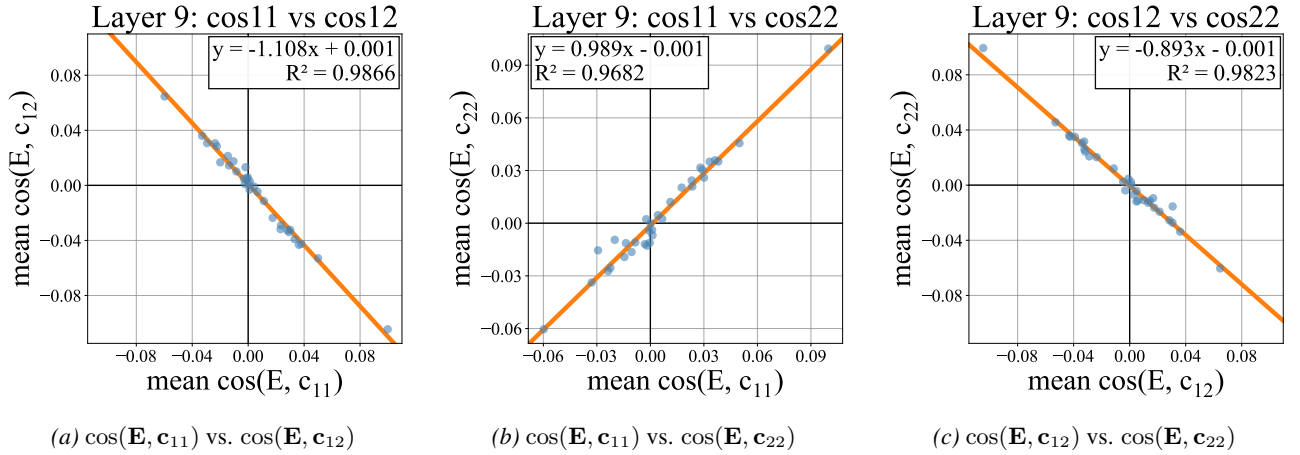


Figure 12. Head-level mean alignment relationships at Layer 9 of *Mistral-7B-Instruct-v0.3* on 2WikiMQA. Each point corresponds to one attention head, positioned by its global mean cosine alignment.

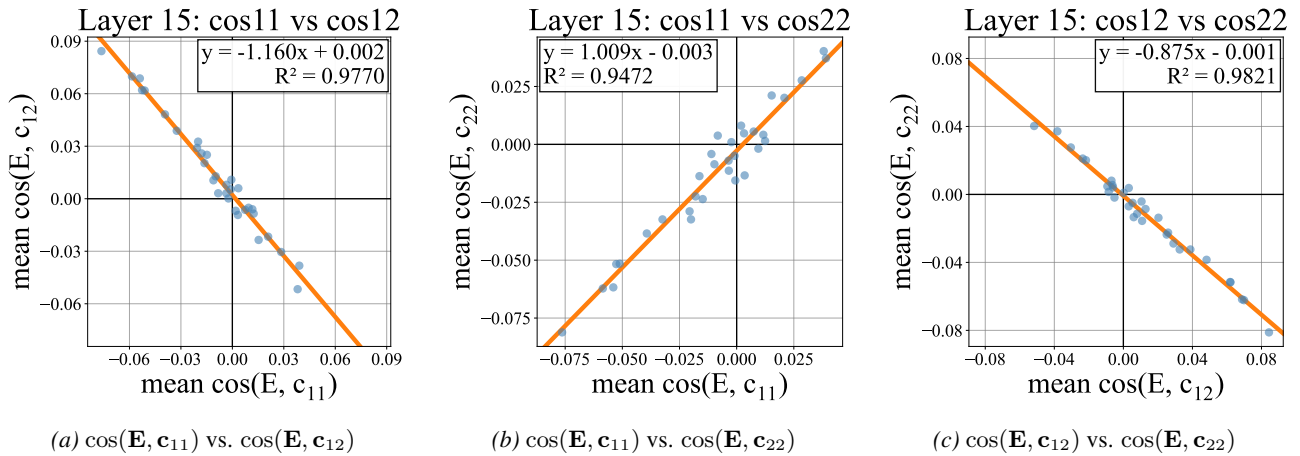


Figure 13. Head-level mean alignment relationships at Layer 15 of *Mistral-7B-Instruct-v0.3* on 2WikiMQA. Each point corresponds to one attention head, positioned by its global mean cosine alignment.

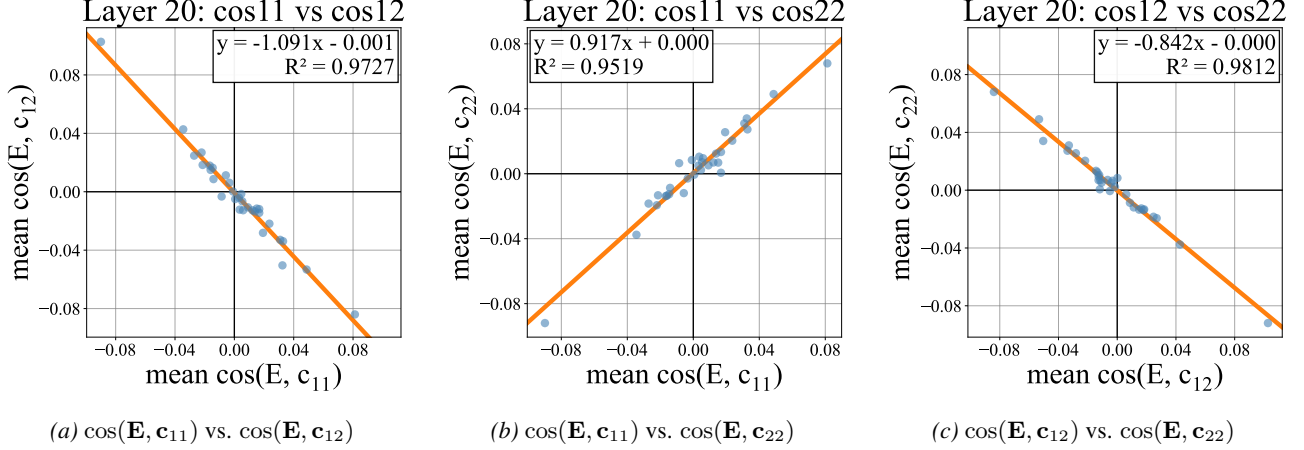


Figure 14. Head-level mean alignment relationships at Layer 20 of *Mistral-7B-Instruct-v0.3* on 2WikiMQA. Each point corresponds to one attention head, positioned by its global mean cosine alignment.

objective through backpropagation; in a statistical sense, it aggregates gradient information across many training samples, positions, and contexts, instead of reflecting an instantaneous reaction to a single token or a single value residual.

Head-external vs. head-internal decomposition of key gradients. By the chain rule, the gradient with respect to a key \mathbf{k}_i is

$$\begin{aligned}
 \frac{\partial L}{\partial \mathbf{k}_i} &= \underbrace{\frac{\partial L}{\partial \mathbf{o}}}_{\text{head-external } \mathbf{E}^\top} \underbrace{\frac{\partial \mathbf{o}}{\partial \alpha_i} \frac{\partial \alpha_i}{\partial z_i} \frac{\partial z_i}{\partial \mathbf{k}_i}}_{\text{head-internal}} \\
 &= \underbrace{\mathbf{E}^\top}_{\text{head-external}} \left(\underbrace{\mathbf{v}_i - \sum_j \alpha_j \mathbf{v}_j}_{\text{head-internal residual } (\mathbf{v}_i - \mathbf{o})} \right) \underbrace{\alpha_i (1 - \alpha_i)}_{\text{head-internal}} \underbrace{\frac{1}{\sqrt{d_k}} \mathbf{q}}_{\text{head-internal common direction}} \\
 &= \frac{\alpha_i (1 - \alpha_i)}{\sqrt{d_k}} \left(\underbrace{\mathbf{E}^\top (\mathbf{v}_i - \mathbf{o})}_{\text{head-external} \times \text{head-internal: scalar projection}} \right) \underbrace{\mathbf{q}}_{\text{head-internal common direction}}. \tag{37}
 \end{aligned}$$

Eq. 37 provides a clear decomposition between *head-external* and *head-internal* factors. Here \mathbf{E} is the head-external gradient propagated from downstream modules and the final loss; it specifies the first-order descent direction of the head output \mathbf{o} under the global training objective, and does not correspond one-to-one to any specific local residual. In contrast, $(\mathbf{v}_i - \mathbf{o})$ is the head-internal residual induced by the current context of this head, and different positions only modulate the update through the scalar projection $s_i = \mathbf{E}^\top (\mathbf{v}_i - \mathbf{o})$.

More importantly, Eq. 37 shows that within the same head, the gradients of all keys \mathbf{k}_i are always colinear with \mathbf{q} ; positional differences appear only in the magnitude $\alpha_i (1 - \alpha_i) s_i$. Near convergence, as the overall gradient magnitude decreases, these local modulation terms become mild: not only is the scale $|s_i|$ suppressed, but the angular variation between \mathbf{E} and the heterogeneous residuals $(\mathbf{v}_i - \mathbf{o})$ also becomes more stable. This aligns with our motivation that $(\mathbf{v}_i - \mathbf{o})$ exhibits intrinsic heterogeneity, while \mathbf{E} acts as a shared, approximately unbiased descent direction that does not favor any specific token residual. Equivalently, \mathbf{E} tends to induce an approximately consistent projection relationship onto the residual subspace across contexts.

(i) $\cos(\mathbf{E}, \mathbf{c}_{11}) \approx \cos(\mathbf{E}, \mathbf{c}_{22})$. Consider the empirical risk objective in Eq. 36. Around a converged solution, the backpropagated signal \mathbf{E} primarily reflects the head output’s first-order descent direction under the global objective, rather than amplifying a particular local position. From Eq. 37, within a head, all key updates share the same head-external factor \mathbf{E} and the common direction \mathbf{q} , while positional differences enter only through $s_i = \mathbf{E}^\top (\mathbf{v}_i - \mathbf{o})$. As the overall gradient magnitude shrinks near convergence, the variation of these projections across neighboring positions is simultaneously

reduced, so the angular relation (i.e., the angle with \mathbf{E}) becomes comparable. Thus, while s_m and s_{m+1} need not be exactly equal, their directional behavior is similar in the sense of cosine alignment.

Next we examine the directional properties of the second-order coefficients. By definition,

$$\mathbf{c}_{11} = \alpha_m(1 - 2\alpha_m)(\mathbf{v}_m - \mathbf{o}), \quad \mathbf{c}_{22} = \alpha_{m+1}(1 - 2\alpha_{m+1})(\mathbf{v}_{m+1} - \mathbf{o}), \quad (38)$$

so \mathbf{c}_{11} and \mathbf{c}_{22} are exactly parallel to their corresponding local residuals $\mathbf{v}_m - \mathbf{o}$ and $\mathbf{v}_{m+1} - \mathbf{o}$, differing only by scalar factors. In our merging strategy, we only merge adjacent keys with small accumulated attention mass, where typically $\alpha_i < \frac{1}{2}$, hence $\alpha_i(1 - 2\alpha_i) > 0$. This factor is strictly positive and therefore preserves direction, merely rescaling the magnitude. Combining this with the near-convergence stability that \mathbf{E} responds with similar angular behavior across different residuals, we obtain

$$\cos(\mathbf{E}, \mathbf{c}_{11}) = \cos(\mathbf{E}, \mathbf{v}_m - \mathbf{o}), \quad \cos(\mathbf{E}, \mathbf{c}_{22}) = \cos(\mathbf{E}, \mathbf{v}_{m+1} - \mathbf{o}), \quad (39)$$

and consequently,

$$\cos(\mathbf{E}, \mathbf{c}_{11}) \approx \cos(\mathbf{E}, \mathbf{c}_{22}). \quad (40)$$

Sign relation with the off-diagonal softmax Hessian. The softmax Hessian has a fixed sign structure: off-diagonal entries are always negative,

$$\frac{\partial^2 \alpha_i}{\partial z_j \partial z_k} = \begin{cases} \alpha_i(1 - 2\alpha_i), & i = j = k, \\ -\alpha_i \alpha_j, & i \neq j, \end{cases} \quad (41)$$

so the adjacent coupling term in the value space can be written as

$$\mathbf{c}_{12} = -\alpha_m \alpha_{m+1} [(\mathbf{v}_m - \mathbf{o}) + (\mathbf{v}_{m+1} - \mathbf{o})]. \quad (42)$$

Let $\mathbf{r}_m \triangleq \mathbf{v}_m - \mathbf{o}$ and $\mathbf{r}_{m+1} \triangleq \mathbf{v}_{m+1} - \mathbf{o}$. Then

$$\mathbf{c}_{11} = a_m \mathbf{r}_m, \quad \mathbf{c}_{22} = a_{m+1} \mathbf{r}_{m+1}, \quad \mathbf{c}_{12} = -b(\mathbf{r}_m + \mathbf{r}_{m+1}), \quad (43)$$

which shows that \mathbf{c}_{12} is a (negative) linear combination of the two residual directions and lies in the same local residual subspace in value space. Putting the above together yields

$$\cos(\mathbf{E}, \mathbf{c}_{11}) \approx \cos(\mathbf{E}, \mathbf{c}_{22}) \approx -\cos(\mathbf{E}, \mathbf{c}_{12}). \quad (44)$$

This is also consistent with our empirical observations.